Journal of Solid State Chemistry 183 (2010) 2154–2160

Contents lists available at ScienceDirect

Journal of Solid State Chemistry

journal homepage: www.elsevier.com/locate/jssc

A nitrilo-tri-acetic-acid/acetic acid route for the deposition of epitaxial cerium oxide films as high temperature superconductor buffer layers

T.T. Thuy, P. Lommens, V. Narayanan, N. Van de Velde, K. De Buysser, G.G. Herman, V. Cloet, I. Van Driessche *

Department of Inorganic and Physical Chemistry, Ghent University, Krijgslaan 281 - S3, 9000 Gent, Belgium

ARTICLE INFO

Article history:
Received 24 February 2010
Received in revised form
17 June 2010
Accepted 10 July 2010
Available online 15 July 2010

Keywords:
Species distribution simulation
CeO_2 buffer layers
Thin films
Superconductor
Sol–gel
Nitrilo-tri-acetic-acid

ABSTRACT

A water based cerium oxide precursor solution using nitrilo-tri-acetic-acid (NTA) and acetic acid as complexing agents is described in detail. This precursor solution is used for the deposition of epitaxial CeO_2 layers on Ni-5at%W substrates by dip-coating. The influence of the complexation behavior on the formation of transparent, homogeneous solutions and gels has been studied. It is found that ethylenediamine plays an important role in the gelification. The growth conditions for cerium oxide films were Ar-5% gas processing atmosphere, a solution concentration level of 0.25 M, a dwell time of 60 min at 900 °C and 5–30 min at 1050 °C. X-ray diffraction (XRD), scanning electron microscope (SEM), atomic force microscopy (AFM), pole figures and spectroscopic ellipsometry were used to characterize the CeO_2 films with different thicknesses. Attenuated total reflection-Fourier transform infrared (ATR–FTIR) was used to determine the carbon residue level in the surface of the cerium oxide film, which was found to be lower than 0.01%. Textured films with a thickness of 50 nm were obtained.

1. Introduction

The discovery of high temperature superconductors (HTSC) in the late 1980s [1] led to the need to produce homogeneous and high-purity metal oxide species for both superconductors and buffer layers, a need that could be met by the use of sol–gel chemistry [2]. Recently, the second generation HTSC became promising in practical applications and successful deposition of HTSC films on small, single crystal substrates was achieved [3–5]. This inspired the idea of depositing HTSC films on flexible and inexpensive metal tape substrates via low cost coating methods. For example, Sathyamurthy et al. [6] have explored in-depth the use of sol–gel processed epitaxial lanthanum zirconate films as seed and barrier layers, thus simplifying the coated conductor architecture from YBCO/CeO_2/YSZ/Y_2O_3/Ni–W to YBCO/LZO/Ni–W or YBCO/CeO_2/LZO/Ni–W. Such a simplified architecture will render the conductor fabrication route more scalable and cheaper. Presently, scientific research worldwide is focusing on the investigation and improvement of buffer layers and $Y_1Ba_2Cu_3O_x$ (YBCO) superconducting properties as well as low cost manufacturing processes in co-operation with industrial companies [7,8].

Among the metallic substrates, Ni-based alloys are well chosen substrates in the development of long lengths of coated superconductors. They possess a strong cube texture in combination with the appropriate mechanical properties and are inexpensive [9,10]. In order to prevent Ni from diffusing into the superconducting layer and simultaneously to transfer a strong biaxial texture from the substrate to the superconducting layer, intermediate buffer layers are deposited onto Ni-based tapes. Materials such as CeO_2 [11–15], YSZ [16], MgO [17], $La_2Zr_2O_7$ [18] and $SrTiO_3$ [19] are not only chemically but also structurally compatible with high temperature superconducting YBCO. Among the most used buffer materials, CeO_2 in particular represents a considerable challenge because of its insulating properties, remarkable chemical stability and small lattice mismatch. YBCO on top of CeO_2 surfaces will grow with a rotation of 45°, to minimize lattice mismatch [20].

In recent studies, it is shown that CeO_2 films fabricated from cerium acetate precursors in organic solvents exhibit a high texture quality [21]. An aqueous precursor solution, obtainable from inexpensive, environmental friendly and easily available chemicals and displaying good long-term stability has recently been published [22]. This precursor solution uses an ethylenediamine tetra acetic acid (EDTA)/acetic acid method for deposition of epitaxial cerium oxide films as HTSC buffers. The replacement of EDTA by a smaller ligand, i.e. NTA, is being studied in this paper in order to reduce the carbon content in the sol–gel system.

The combination of two complexing compounds (NTA and acetic acid) has been examined in order to establish the preparation of a stable precursor solution which can be used for dip-coating. Simulation programs were employed to build up

* Corresponding author. Fax: +32 9264 4983.
E-mail address: Isabel.Vandriessche@UGent.be (I. Van Driessche).

0022-4596/$ - see front matter © 2010 Elsevier Inc. All rights reserved.
doi:10.1016/j.jssc.2010.07.009

models expressing the influence of their complexation behavior on the formation of transparent and homogeneous precursor solutions and gels. From these stable precursor solutions, cerium oxide buffer layers were deposited. The CeO_2 layers were characterized using XRD and pole figures for phase purity and texture, SEM for homogeneity and microstructure, spectroscopic ellipsometry for the thicknesses of the films and AFM for surface roughness analysis. ATR–FTIR has been used to determine the carbon content of the surface of cerium oxide films.

2. Experimental

2.1. Chemicals

Cerium acetate $Ce(OAc)_3$, ethylenediamine (EDA), nitrilo-triacetic acid (NTA), NaCl and Na_2CO_3 were purchased from Sigma-Aldrich (Germany). Glacial acetic acid (99 wt%) was obtained from Chem.-Lab (Belgium). Thermo gravimetric analysis/differential thermal analysis (TGA/DTA) was performed on the starting cerium acetate to determine the water content in order to assure the concentration and the ratio of cerium to ligands in the precursor solution.

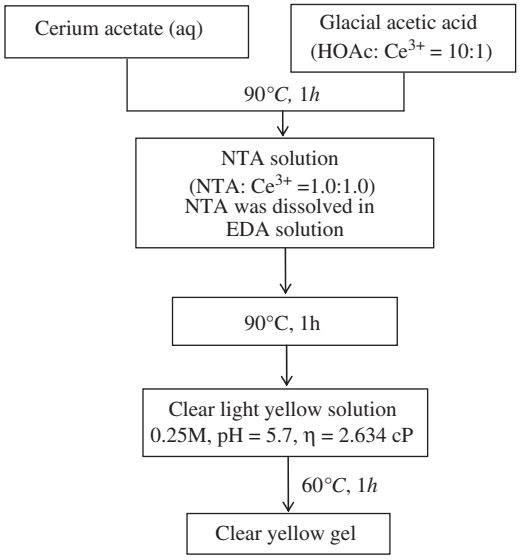

Fig. 1. Schematic overview of the aqueous CeO_2 precursor solution route.

2.2. HySS program

The hyperquad simulation and speciation (HySS) program provides a system for simulating titration curves and providing speciation diagrams [23,24]. HySS thereby provides an integrated environment for setting up calculations and performing them, resulting in the distribution diagrams of the species present in solution. There are no limits imposed on the number of reagents, complexes or partially soluble products that may be present. Three types of measurements were performed using the program: (i) simulation of the titration curves, (ii) calculation of species' concentrations for a range of conditions and (iii) speciation for a single set of conditions.

The results of the calculations lead to information on equilibria present in the solution and the presence of soluble and non-soluble species. The HySS program thereby provides information on the influence of the type of complexing agents chosen, the combination of complexing agents and their ratio to the metal concentration necessary to obtain stable and clear solutions. It also helps in predicting the pH range in which the free concentration of the metal ions can be kept minimal to obtain a clear solution. The HySS program therefore provides a useful method to guide the experiments.

Data input of the HySS program allows equilibrium constants, solubility products and/or stoichiometric coefficients to be entered. In our case, details about the initial concentrations of Ce^{3+}, acetic acid, EDA and NTA are added in the simulation. Specifying the initial and final pH further defines the range over which the speciation calculation is to be performed. This paper describes the simulation for molar ratios between Ce(III):acetic acid:NTA of 1:10:1 for a pH range from 1 to 11. The stability constant data needed for that purpose were taken from the literature [25,26].

2.3. Solution and film synthesis

The scheme used to prepare the CeO_2 precursor solution is shown in Fig. 1. Cerium acetate was dissolved in a mixture of water and acetic acid with a stoichiometric ratio Ce^{3+}: acetic acid of 1:10. This solution was added to an EDA solution in which NTA is dissolved in its acidic form (Ce^{3+}: NTA ratio of 1:1). The final pH of the solution was adjusted by EDA up to a value between 5.5 and 6.2. The combination of these ligands leads to a clear and homogeneous sol and gel as shown in Fig. 2. The solutions could be stored at room temperature for several months without losing their stability.

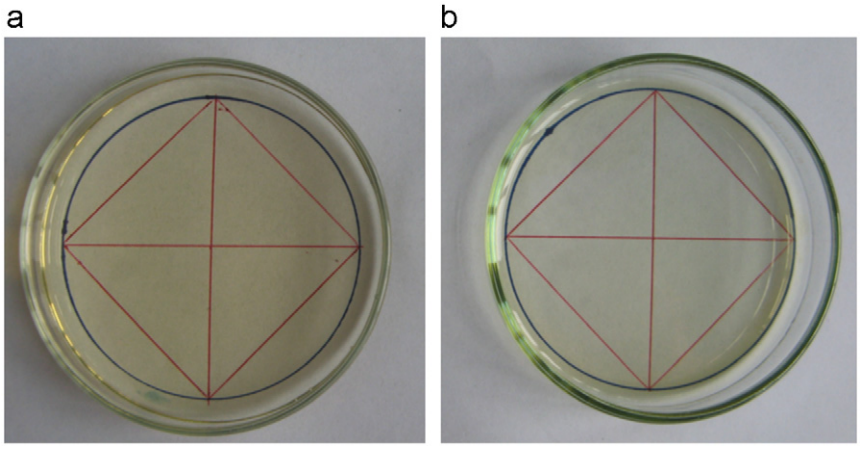

Fig. 2. Pictures of clear and homogeneous sol (a) and gel (b).

The Ni–5 at%W tape was cut into strips of approximately 2 cm in length. The cleaning procedure of Ni tapes was described in detail elsewhere [22]. The films were prepared by dip-coating at room temperature in a clean room (class 10000) with a computer controlled precision dip-coater. After the substrates were dipped into solutions with a cerium concentration of 0.25 M, they were held immersed for 10 s and then withdrawn at 10–40 mm/min.

The dip-coated samples were converted into gels in a dust free furnace for 1 h at 60 °C. Subsequently, these amorphous gels were transformed into the desired crystalline CeO_2 phase by an appropriate heat treatment in a quartz tube furnace under Ar-5% H_2 processing atmosphere, a dwell time of 60 min at 900 °C and 5–30 min at 1050 °C.

2.4. Characterization

The thermal decomposition behavior of the gel network was studied by TGA–DTA (STD 2960 simultaneous DSC-TGA). The CeO_2 layers were characterized using X-ray diffraction (Siemens D5000, Cu$K\alpha$) and pole figures for phase purity and texture (Bruker D8, SOL-X energy dispersive detector), SEM (Philips 501) for homogeneity and microstructure, AFM, Molecular Imaging Picoplus (PicoScan 2100 Controller) for surface roughness analysis and spectroscopic ellipsometry (JA Woollam Alpha-SE) for the thickness of the films. Attenuated total reflection/Fourier transform infrared spectroscopy (ATR/FTIR, Perkin Elmer 160 FT-IR) was used for analysis of the carbon residue in the cerium oxide thin films.

3. Results and discussion

3.1. Precursor solutions

In order to obtain high quality layers we need to start from a clear and stable precursor solution which can be transformed into a homogeneous gel upon solvent evaporation. Reasonably thick films require a high Ce^{3+} concentration. Cerium (III) acetate is only slightly soluble in water and has an inverse temperature solubility relationship. It will dissolve to about 115 g/L at 15 °C, but the solubility falls to 100 g/L at 25 °C [27]. Therefore, we need to add an additional chelating agent to the solution. When a ligand is introduced to a solution containing metal ions, the concentration of free metal ions in solution is reduced dramatically by the formation of water soluble chelate complexes [28]. Furthermore, free concentration of metal ions is not high enough to get precipitates upon the solvent evaporation.

We first optimized the formulation of the cerium precursor by varying the pH value and the molar ligand-to-metal-ratio. At the same time, the organic content was kept as low as possible. The cerium precursor solution was prepared by dissolving cerium acetate in a mixture of acetic acid and water. The concentration of acetic acid was varied from 12 to 20 vol%. The acidity of the obtained solutions is decreased by adding ethylenediamine up to a pH value of 6. Only the solutions containing at least 14 vol% of acetic acid are completely free of precipitates.

In our recently published article, EDTA was introduced as chelating agent to stabilize Ce^{3+} in solution. Clear sols and gels could be obtained [22]. However, highly textured CeO_2 layers with a thickness of only 35 nm were obtained. In order to obtain a thicker CeO_2 film, a higher density of cerium is required compared to CeO_2 precursor solutions using EDTA as complexant. Therefore, EDTA needs to be replaced by a smaller ligand of lower molecular weight. Among the complexing agents for rare earth elements such as nitrilo-tri-acetic (NTA), diethylenetriaminepentaaceticacid (DTPA), trans-1,2-diaminocyclohexanetetraacetic (DCTA), bis-(aminoethyl)-glycolether-N, N, N′, N′ tetra acetic (EGTA), NTA has a low molecular weight [29,30].

NTA forms complexes with Ce^{3+} in the ratios 1:1 and 2:1 according to the following reactions [26]:

$$Ce^{3+} + NTA \leftrightharpoons [Ce(NTA)] \quad \log\beta = 10.70$$

$$Ce^{3+} + 2NTA \leftrightharpoons [Ce(NTA)_2]^{3-} \quad \log\beta = 18.66$$

Like EDTA, NTA in acid form is sparingly soluble in water. The neutralization of NTA with weak bases like ammonia or ethylenediamine (EDA) to pH 6 allows the preparation of a NTA solution in a higher concentration range. NTA was added in different molar ligand-to-metal-ratios (from 0.7 to 1.5) to improve the formation of a clear, transparent and stable gel. The minimal amount of NTA leading to highly stable solutions and gels was at a molar ratio between NTA and metal ions of 1:1.

During this study, the possibility was also examined to prepare a CeO_2 precursor solution using cerium acetate, acetic acid and NTA, where NTA was dissolved in an ammonium hydroxide solution. The solution was clear but it is not stable for more than a few days. Furthermore, there are precipitates present after gelification. However, the replacement of ammonia by EDA resulted in clear and stable solutions and gels. Two important differences between ammonia and EDA might explain this change in stability for both solutions and gels. First, EDA has a much higher boiling point than NH_3 (116 °C for EDA and 36 °C for ammonium hydroxide with 10–30% NH_3) and thus NH_3 might evaporate much faster causing important variations of the pH. Second, in contrast to ammonia, the two amine functional groups of EDA can react with the carboxylic group of NTA with the formation of a polyamide. This polyamide might further stabilize the Ce(III) ions forming a continuous network in the gel.

3.2. Characterization of the precursor solutions by the HySS program

The HySS program was used to calculate the equilibrium concentration of all species present in the solutions. The model allows entering of the equilibrium constants, solubility products and/or stoichiometric coefficients. With an identical molar ratio of Ce^{3+}:acetic acid:EDA (1:10:1), the distribution of the different species was calculated by using the stability constants from literature. The initial concentrations of Ce^{3+}, acetate and NTA in the simulation were 0.2, 2.0 and 0.2 M, respectively. The detailed model of species used in HySS is shown in Table 1. The results of the simulation are shown in Fig. 3. One can see that at low pH (pH=2.5), cerium is coordinated by NTA and a maximum amount

Table 1
The stability constant data of Ce^{3+} with acetic acid and NTA taken from Refs. [21,22] used as model for the HySS program.

Species	log beta	Ce^{3+}	OAc^-	NTA^{3-}	H
HOAc	4.56	0	1	0	1
$HNTA^{2-}$	9.65	0	0	1	1
H_2NTA^-	12.13	0	0	1	2
H_3NTA	13.93	0	0	1	3
H_4NTA^+	13.93	0	0	1	4
$[Ce(OAc)]^{2+}$	1.91	1	1	0	0
$[Ce(OAc)_2]^+$	3.09	1	2	0	0
$[Ce(OAc)_3]$	3.68	1	3	0	0
[Ce(NTA)]	10.70	1	0	1	0
$[Ce(NTA)_2]^{3-}$	18.66	1	0	2	0
$Ce(OH)_3$	−19.70	1	0	0	−3
OH^-	−13.78	0	0	0	−1

The compositions of species are given with stoichiometric coefficients. A negative coefficient for H means bonded OH^-.

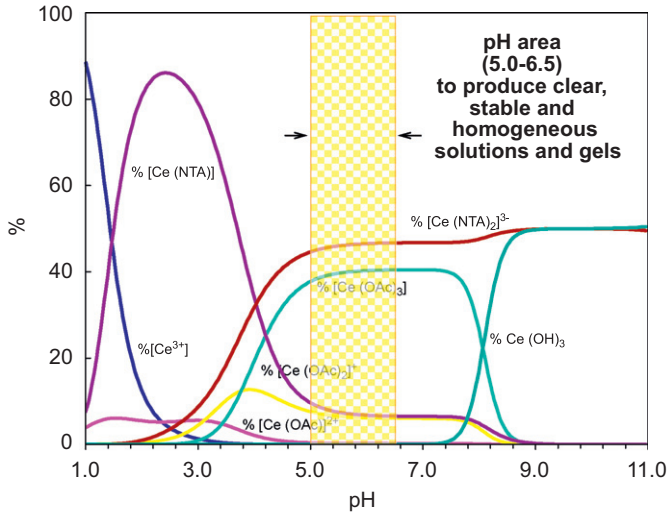

Fig. 3. Simulated distribution of species for a solution containing Ce^{3+}, acetic acid, EDA, and NTA at 25 °C, I = 0.1 M (with Ce^{3+}: acetic acid: NTA = 1:10:1).

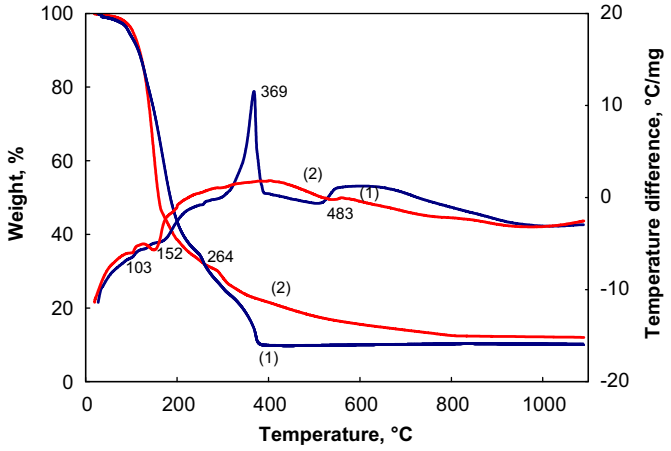

Fig. 4. TGA-DTA curves for decomposition of cerium precursor gels in air (1) and Ar (2) atmosphere with a heating rate of 10 °C/min.

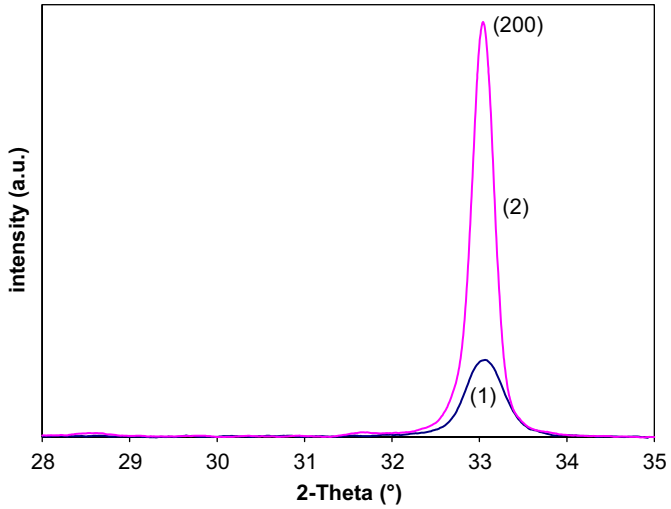

Fig. 5. XRD of CeO_2 thin films on Ni-W tape. (1) film 10 nm, (2) film 50 nm.

of [Ce(NTA)] (86%) is obtained. The concentration of free Ce^{3+} ions is significantly reduced from 88% to 1% at pH 3.0. In contrast to Ce–EDTA complexes, NTA tends to form 2:1 (ligand:metal) complexes with Ce^{3+} at higher pH. In this case 46% of the cerium atoms are present as $[Ce(NTA)_2]^{3-}$ complexes at a pH of 5.0, while the presence of [Ce(NTA)] is merely 8%. The expected progressive formation of the $[Ce(OAc)_3]$ is detected from pH 3 onwards. In the pH range 5.0–7.4, $[Ce(OAc)_3]$ and $[Ce(NTA)_2]^{3-}$ are the governing species. Upon moving into the alkaline region $Ce(OH)_3$ starts to precipitate. We can conclude from this that the optimal pH range of the precursor solution is 5.0–6.5 which is in agreement with the experimental results.

3.3. Characterization of the gels

The thermal decomposition behavior of the cerium precursor gels was studied in order to establish a suitable heat treatment

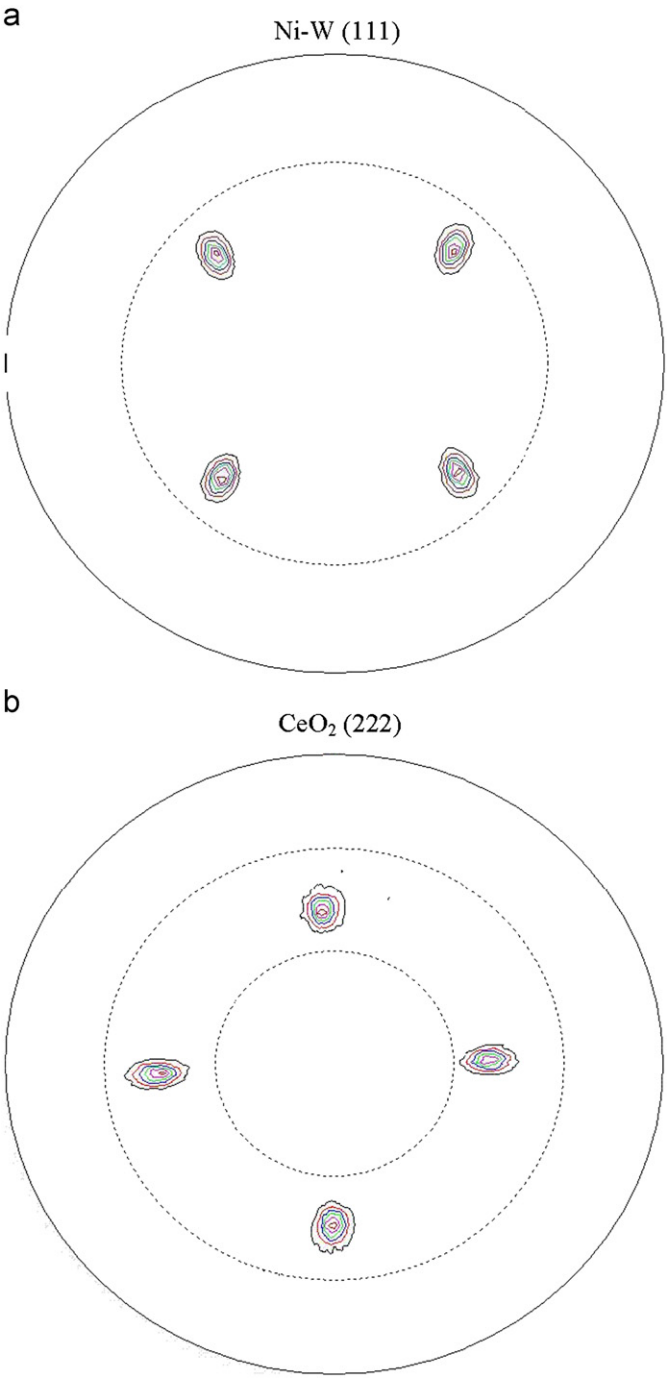

Fig. 6. X-ray pole figures of (a) Ni-W (111) and (b) CeO_2 on a Ni-W substrate.

schedule. Fig. 4 shows the TGA–DTA curves in air and Ar for CeO_2 precursor gels in the range from 25 to 1100 °C. At temperatures below 200 °C, two large decomposition steps occur at 100 and 150 °C in rapid succession. These two steps can be associated with the release of water and acetic acid [7]. They are followed by escape of gases such as CO_x, NO_x at temperatures ranging from 200 to 500 °C due to the decomposition of the gel. The escape of CO gas may occur at 483 °C which is in agreement with the thermal decomposition of cerium acetate hydrate reported by Arri et al. [31]. The mass loss of the gel in air and in Ar is almost the same from room temperature until 300 °C. However, from a temperature of 264 °C on, the mass loss of the gel measured under Ar decreased much more than the one in air. As can be seen from the TGA curve, there is no mass loss above 800 °C, the temperature at which cerium oxide is being formed. This is in agreement with the early nucleation and growth analysis by in situ high temperature XRD [21].

3.4. Characterization of CeO_2 films

3.4.1. Microstructure and morphology

The θ–2θ scans of the CeO_2 films made with a dip-coat speed of 10 and 40 mm/min are shown in Fig. 5. The thicknesses of the films are 10 and 50 nm, respectively.

The thickness of the films was calculated from spectroscopic ellipsometry measurements by fitting the parameters (wavelength=632.8 nm and refractive index=1.887) of a reference (with known thickness) CeO_2–NiW model [32]. The growth conditions for cerium oxide films from NTA based solution are: Ar–5% H_2 gas processing atmosphere, a ramp of 5 °C/min to 900 °C, a dwell time of 60 min at 900 °C and another ramp of 10 °C/min to 1050 °C with dwell time range 5–30 min at 1050 °C. This thermal treatment was also successfully applied to the deposition of cerium oxide onto the Ni–W using water based precursor with EDTA [22].

The strong CeO_2 (2 0 0) reflections and the absence of non-(h 0 0) reflections indicate that the CeO_2 layers have a strong cube texture. A weak feature observed around 2 theta 28.5° is due to a very small fraction of (1 1 1) CeO_2 still present in the sample.

The intensity of the (2 0 0) reflections mainly depends on the thickness of the films. The thicker films also seem to have a lower full-width-at-half-maximum (FWHM), which means the thicker films are more crystalline than the thinner films (Fig. 5). The thick film has a FWHM of 0.32° and the thin film has a FWHM of 0.57°.

To examine the in-plane orientation of a CeO_2 buffer layer on Ni–W, (1 1 1) pole figures were measured on a treated Ni–W and a CeO_2 film. Fig. 6 compares the (1 1 1) NiW pole figure to the (2 2 2) CeO_2 pole figure. An angle of 54.6° (Ψ) was used to acquire both the pole-figures. The CeO_2 buffer layer shows a very good in-plane alignment (Φ-scan) with a FWHM value of 6.67° (Ni: 6.00°). This means that an epitaxial CeO_2 film has been formed onto the biaxially textured Ni–W tape. The results are shown in Fig. 7.

Rocking curve analysis of CeO_2 (2 0 0) reveals an out-of-plane orientation ω=8.32°. This value will be further optimized in another paper by improving the thermal process and substituting Ce with other elements.

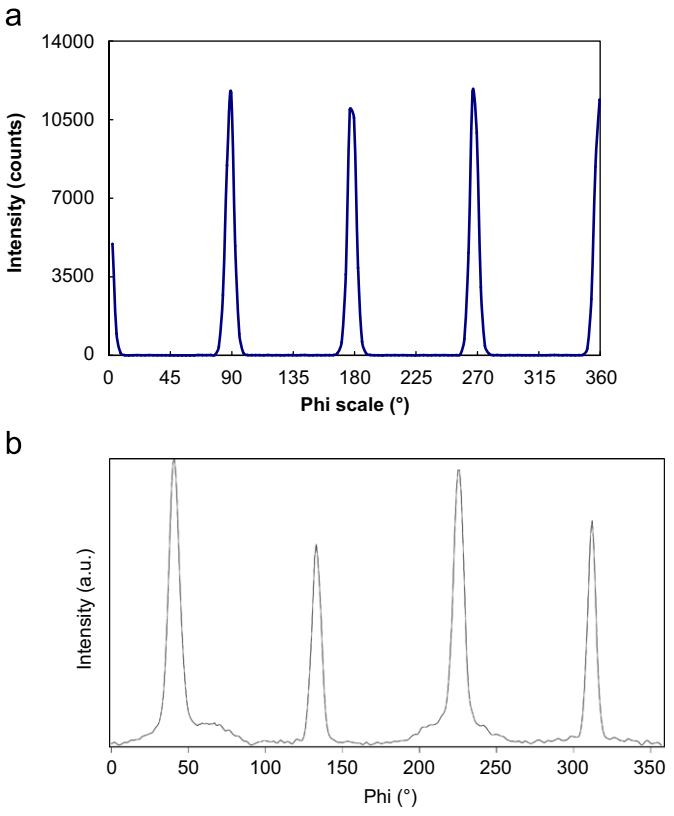

Fig. 7. Phi scans of Ni–W and a CeO_2 buffer layer on a Ni–W substrate. (a) Ni(111) FWHM 6.00 and (b) CeO_2 (222) FWHM 6.67.

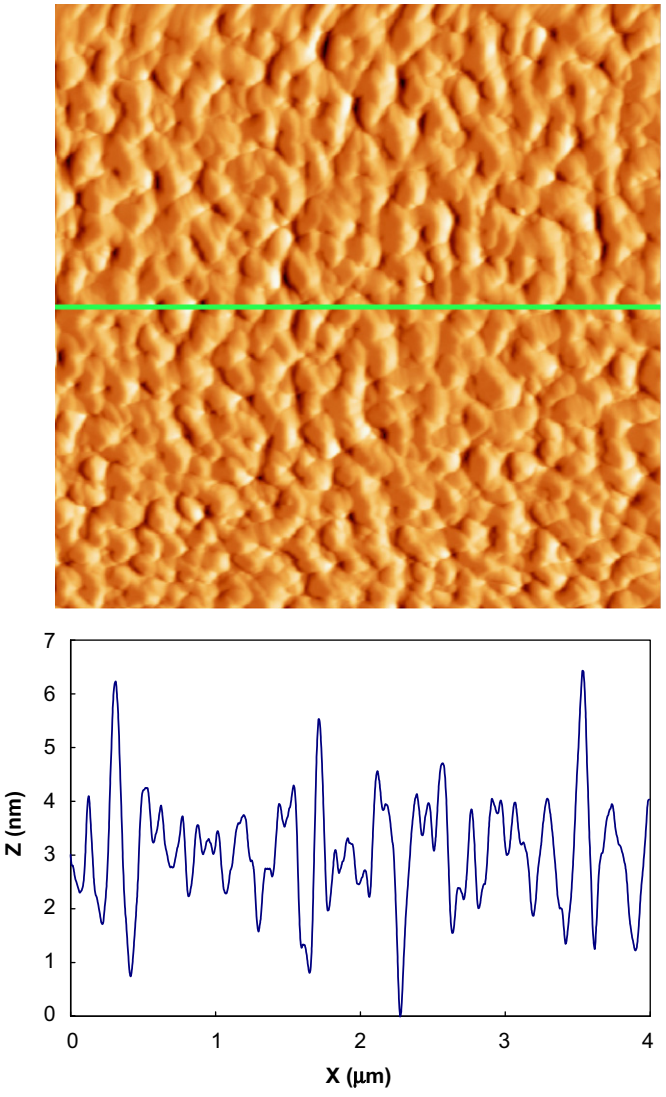

Fig. 8. AFM micrograph of CeO_2 with thickness 50 nm in 2d (4 * 4 μm) and the average roughness of 5.0 nm.

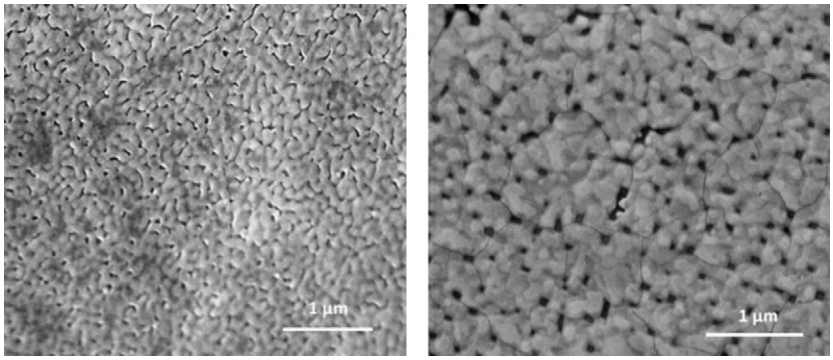

Fig. 9. SEM micrographs of CeO_2 films with thickness of 10 nm and 50 nm.

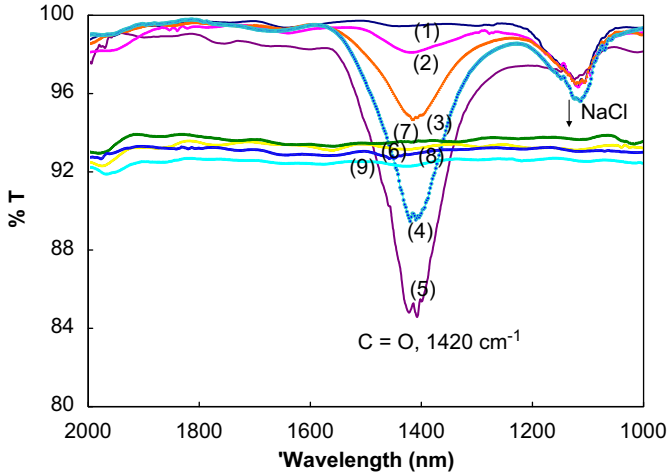

Fig. 10. ATR-FTIR data used to determine carbon residue in the surface of CeO_2 thin films. (1) NaCl, (2) 0.01% carbon in NaCl, (3) 0.03% carbon in NaCl, (4) 0.06% carbon in NaCl, (5) 0.11% carbon in NaCl, (6) CeO_2-EDTA 10nm, (7) CeO_2-EDTA 50 nm, (8) CeO_2-NTA 10 nm, (9): CeO_2-NTA 50 nm.

AFM micrographs of a CeO_2 buffer layer with thickness of 50.0 nm are presented in Fig. 8. SEM micrographs of the CeO_2 films with thicknesses of 10.0 and 50.0 nm are presented in Fig. 9. These micrographs indicate a smooth surface morphology. The average roughness is around 5.0 nm (scanned area: 16 μm^2). By improving the thermal treatment and substituting Ce, we have the intention to further improve the density and flatness of the surface.

3.4.2. *Carbon residue in the CeO_2 surface thin films*

In this study, ATR–FTIR was used to verify the assumption of low carbon residue using water based precursors (Fig. 10). The IR high frequency region (2800–3000 cm^{-1}) and lower frequency region (1600–1200 cm^{-1}) were examined. The reflection at 2800–3000 cm^{-1} is typical for C–H stretching, showing the remainders of organic compounds from the precursor or contaminants from the environment. Since the samples have been treated at high temperatures, it is to be expected that no traces of these materials were left, which was also experimentally proven.

The analysis here focused mainly on the presence of cerium carbonate and carbonates in general, since these materials can be expected to form at higher temperatures as decomposition products of the water based precursors or as common contaminant of oxide surfaces. Since these carbonates are very stable at higher temperatures, a study of their presence was undertaken to make sure that no traces were left.

If the cerium oxide film would contain carbonate residues, a signal due to C=O stretch in the region of 1400–1500 cm^{-1} is expected [33]. The sensitivity of the used ATR/FTIR spectrometer was determined to be 0.01% (as established for the detection of the C=O stretch of sodium carbonate at 1420 cm^{-1} [34,35] in a matrix of sodium chloride). However, when analyzing the cerium oxide film surfaces (Fig. 10), no evidence for a C=O stretch could be detected in this region. Hence, the level of carbonate residue in the cerium oxide films is assumed to be lower than 0.01%.

4. Conclusion

We have successfully synthesized a water based cerium acetate precursor for the deposition of textured CeO_2 coatings. This precursor is very stable, environmental friendly and leaves less carbon residue ($<0.01\%$) compared to precursors based on organic solvents. The influence of complexation behavior on the formation of transparent and homogeneous sols and gels has been studied and interpreted using simulated metal–ligand distributions calculated equilibriums with the HySS program. The occurrence of different species at different pH values could be related to stable gel formation conditions. This novel sol–gel system was successfully applied for the deposition of epitaxial CeO_2 films on Ni 5 at%W substrates by dip-coating. Highly textured CeO_2 layers with a thickness up to 50 nm were obtained.

Acknowledgments

The authors would like to acknowledge the help of D. Vandeput (Ghent University) for AFM measurements, J. Caroen (Ghent University) for ATR–FTIR measurements, O. Janssen (Ghent University) for the XRD, SEM and pole figure measurements, M. Bäcker (Zenergy Power, GmbH) for providing us with Ni–W tape and T. Wagner (Lot-Oriel Company) for spectroscopic ellipsometry measurements.

References

[1] M.K. Wu, J.R. Ashburn, C.J. Torng, P.H. Hor, R.L. Meng, L. Gao, Z.J. Huang, Y.Q. Wangand, C.W. Chu, Phys. Rev. Lett. 58 (1987) 908–910.
[2] J.A. Crayston, in: Sol-Gel, Comprehensive Coordination Chemistry II, Pergamon, Oxford, 2004.
[3] M. Falter, W. Häßler, B. Schlobach, B. Holzapfel, Phys. C: Superconductivity 372-376 (2002) 46–49.
[4] J.M. Dekkers, G. Rijnders, S. Harkema, H.J.H. Smilde, H. Hilgenkamp, H. Rogalla, D.H.A. Blank, Appl. Phys. Lett. 83 (2003) 5199–5201.
[5] Z. Ye, Q. Li, W.D. Siand, P.D. Johnson, IEEE Trans. Appl. Supercon. 15 (2005) 3013–3015.
[6] S. Sathyamurthy, M. Paranthaman, H.Y. Zhai, S. Kang, T. Aytug, C. Cantoni, K.J. Leonard, E. Payzant, H.M. Christen, A. Goyal, J. Mater. Res. 19 (2004) 2117–2123.

[7] V. Cloet, M.C. Cordero-Cabrera, T. Mouganie, B.A. Glowacki, M. Falter, B. Holzapfel, J. Engell, M. Bäcker, I. Van Driessche, Adv. Sci. Technol. 47 (2006) 153–158.
[8] K. Knoth, S. Engel, C. Apetrii, M. Falter, B. Schlobach, R. Hühne, S. Oswald, L. Schultz, B. Holzapfel, Curr. Opin. Solid State Mater. 10 (2006) 205–216.
[9] S.S. Kim, J.S. Tak, S.Y. Bae, J.K. Chung, L.S. Alin, C.J. Kim, K.W. Kim, K.K. Cho, Physica C 463 (2007) 604–608.
[10] V. Subramanya Sarma, B. de Boer, J. Eickemeyer, B. Holzapfel, Scr. Mater. 48 (2003) 1167–1171.
[11] Y.-K. Kim, J. Yoo, K. Chung, X. Wang, S.X. Dou, Mater. Lett. 63 (2009) 800–802.
[12] D.E. Wesolowski, M.J. Cima, J. Mater. Res. 21 (2006) 1–4.
[13] M.S. Bhuiyan, M. Paranthaman, S. Sathyamurthy, T. Aytug, S. Kang, D.F. Lee, A. Goyal, E.A. Payzant, K. Salama, Supercond. Sci. Technol. 16 (2003) 1305–1309.
[14] M. Coll, J. Gazquez, R. Huehne, B. Holzapfel, Y. Morilla, J. Garcia-Lopez, A. Pomar, F. Sandiumenge, T. Puig, X. Obradors, J. Mater. Res. 24 (2009) 1446–1455.
[15] V.F. Solovyov, D. Abraimov, D. Miller, Q. Li, H. Wiesmann, J. Appl. Phys. 105 (2009) 113927.
[16] P. Amézaga-Madrid, W. Antúnez-Flores, I. Monárrez-García, J. González-Hernández, R. Martínez-Sánchez, M. Miki-Yoshida, Thin Solid Films 516 (2008) 8282–8288.
[17] T. Izumi, N. Hobara, K. Kakimoto, T. Izumi, K. Hasegawa, M. Kai, T. Honjo, X. Yao, H. Fuji, Y. Nakamura, Y. Shiohara, Phys. C: Superconductivity 357-360 (2001) 1027–1033.
[18] S. Engel, R. Hühne, K. Knoth, A. Chopra, N.H. Kumar, V.S. Sarma, P.N. Santhosh, L. Schultz, B. Holzapfel, J. Cryst. Growth 310 (2008) 4295–4300.
[19] S. Chen, Z. Sun, K. Shi, S. Wang, J. Meng, Q. Liu, Z. Han, Phys. C: Superconductivity 412-414 (2004) 871–876.
[20] X.D. Wu, R.C. Dye, F.E. Muenchausen, S.R. Foltyn, M. Maley, A.D. Rollett, A.R. Garcia, N.S. Nogar, Appl. Phys. Lett. 58 (1991) 2165–2167.
[21] M.S. Bhuiyan, M. Paranthaman, K. Salama, Supercond. Sci. Technol. 19 (2006) R1–R21.
[22] T.T. Thuy, S. Hoste, G.G. Herman, N. Van de Velde, K. De Buysser, I. Van Driessche, J. Sol-Gel Sci. Technol. 51 (2009) 112–118.
[23] P. Gans, A. Sabatini, A. Vacca, Talanta 43 (1996) 1739–1753.
[24] L. Alderighi, P. Gans, A. Ienco, D. Peters, A. Sabatini, A. Vacca, Coordin. Chem. Rev. 184 (1999) 311–318.
[25] A.E. Martell, R.M. Smith, Critical Stability Constants, vol 2, Plenum Press, New York, 1975.
[26] R.M. Smith, A.E. Martell, Critical Stability Constants, vol 3, Plenum Press, New York, 1977.
[27] B. Kilbourn, in: Part 1, A–L. A lanthanide lantology, Molycorp Inc., Mountain Pass, 1993.
[28] M. Kakihana, J. Sol-Gel Sci. Technol. 6 (1996) 7–55.
[29] S. Alfared, F. Zantuti, Y.S. Krylov, J. Radioanal. Nucl. Chem. Ar. 125 (1988) 381–391.
[30] D.C. Harris, in: Quantitative Analytical chemistry, W. H. Freeman, New York, 2006.
[31] T. Arii, A. Kishi, M. Ogawa, Y. Sawada, Anal. Sci. 17 (2001) 875–880.
[32] H.G. Tompkins, W.A.M. Gahan, in: Spectroscopic ellipsometry and reflectometry, a user's guide, John Wiley & Sons, Inc, 1999.
[33] A. Scott, J.E. Gray-Munro, Thin Solid Films 517 (2009) 6809–6816.
[34] F.R. Dollish, W.G. Fateley, F.F. Bentley, in: Characteristic Raman frequencies of organic compounds, Wiley Interscience, 1974.
[35] G. Socrates, in: Infrared and Raman Characteristic Group Frequencies: Tables and Charts, John Wiley & Sons, 2001.